Available online at BCREC website: https://bcrec.id

Bulletin of Chemical Reaction Engineering & Catalysis, 14 (2) 2019, 404-412

Research Article

# Facile Template In-Situ Fabrication of $ZnCo_2O_4$ Nanoparticles with Highly Photocatalytic Activities under Visible-Light Irradiation

**Vu T. Tan[1*], La The Vinh[1], Tran Ngoc Khiem[2], Huynh Dang Chinh[1]**

*[1]School of Chemical Engineering, Hanoi University of Science and Technology, 1, Dai Co Viet, Bach Khoa, Hai Ba Trung, 10000, Ha Noi, Viet Nam*
*[2]International Training Institute for Materials Science (ITIMS), Hanoi University of Science and Technology, 1, Dai Co Viet, Bach Khoa, Hai Ba Trung, 10000, Ha Noi, Viet Nam*

*Received: 15th November 2018; Revised: 15th February 2019; Accepted: 15th February 2019; Available online: 30th April 2019; Published regularly: 1st August 2019*

**Abstract**

High specific surface area $ZnCo_2O_4$ nanoparticles were prepared via a sacrificial template accelerated hydrolysis by using nanoparticles of ZnO with highly polar properties as a template. The obtained $ZnCo_2O_4$ nanoparticles were characterized by the method of scanning electron microscopy (SEM), X-ray diffraction (XRD), Brunauer-Emmett-Teller (BET) surface area measurements, Transmission electron microscopy (TEM), Raman spectroscopy, and X-ray photoelectron spectroscopy (XPS). The obtained nanoparticles were performed as a photocatalyst for the degradation of methylene blue in aqueous solution under visible irradiation. The photocatalytic degradation rate of methylene blue onto the synthesized $ZnCo_2O_4$ was higher than that of commercial ZnO and synthesized ZnO template. 

***Keywords***: Sacrificial template; $ZnCo_2O_4$; photodegradation; methylene blue; ZnO

***How to Cite***: Tan, V.T., Vinh, L.T., Khiem, T.N., Chinh, H.D. (2019). Facile Template In-Situ Fabrication of $ZnCo_2O_4$ Nanoparticles with Highly Photocatalytic Activities under Visible-Light Irradiation. *Bulletin of Chemical Reaction Engineering & Catalysis*, 14(2): 404-412 (doi:10.9767/bcrec.14.2.3613.404-412)

***Permalink/DOI***: https://doi.org/10.9767/bcrec.14.2.3613.404-412

## 1. Introduction

In recent years, the removal of hazardous materials such as toxic dyes and organic residuals in wastewater becomes very attractive [1-3]. Methylene blue (MB) is an organic dye with extensively used for many application fields such as cosmetic, paper, textile, culture, and pharmaceutical purpose [4]. The untreated methylene blue from these industries strongly affects both land and water bodies. Up to now, photocatalysis is a useful method for dye removal which efficiently converts hazardous materials into carbon dioxide and harmless compounds.

Recently, $TiO_2$ and ZnO are two semiconductors which are the most widely used photocatalysts because of their non-toxicity, cost-effectiveness [5-8]. Also, many researchers have reported that ZnO shows better catalytic activity in the degradation of some organic compounds compared to that of $TiO_2$, especially in the visible light region [9-11]. However, ZnO presents a tendency of aggregation and low spe-

* Corresponding Author.
E-mail: tan.vuthi@hust.edu.vn (V.T. Tan);
Telp: +34 98 337 1922

cific surface area which decrease its photocatalytic efficiency [12]. Besides, the photocorrosion of ZnO can occur due to the self-oxidation reactions of ZnO with the holes $h^+$ in the presence of water:

$$ZnO + 2h^+ + nH_2O \rightarrow Zn(OH)_n^{(2-n)+} + \tfrac{1}{2}O_2 + nH^+ \quad (1)$$

$$ZnO + 2h^+ \rightarrow Zn^{2+} + \tfrac{1}{2}O_2 \quad (2)$$

Numerous researches have intensively been investigated to overcome these disadvantages and to enhance the photocatalytic activity of ZnO, such as: combining ZnO with other semiconductors [13-15], transition metals [16], covering ZnO with a transparent thin film using PANI [17], polysilane [12], or combining with noble metals such as: Ag [18] and Pt [19]. However, there are several limitations due to its wide band gap (>3.2 eV) even with doping material which means that the material can be only active at the ultraviolet region.

Recently, spinel compounds with the general formula $AB_2O_4$ is a novel series of mixed metal oxides, with extensively used in many applications, such as: electronic, biotechnology, sensing, catalyst, and energy storage [20]. The A-site generally occupied by divalent cations, such as: Mg, Mn, Ni, or Zn and which is tetrahedrally coordinated in the molecular geometry. Meanwhile, the B-site is commonly trivalent cations (Al, Cr, Co, and Fe) with octahedrally coordinated in the molecular geometry.

Mainly, nanostructure $ZnCo_2O_4$ spinel compound presents a potential application in the gas sensor, anode material, catalyst due to its unique electronic structure properties [21]. To the best of our knowledge, $ZnCo_2O_4$ offers high photocatalytic efficiency for organic pollutants in the visible region [22]. However, the synthesis of $ZnCo_2O_4$ nanoparticles always presents several drawbacks such as the high pressure, the high temperature of synthesis, multi-steps which inhibit its practical application.

In this work, we would like to present a simple novel route to fabricate the $ZnCo_2O_4$ nanoparticles through the template ZnO according to the sacrificial template hydrolysis template (STAH) [23]. For the first time, the photocatalytic efficiency of the synthesized $ZnCo_2O_4$ by STAH method was tested by the photocatalytic degradation of Methylene blue (MB) dye under visible irradiation. The result of this work demonstrates that the fabrication method for $ZnCo_2O_4$ with enhanced photocatalytic activities in the visible light region could provide new comprehension about the fabrication of photocatalytic nanoparticles for environmental pollution control.

## 2. Materials and Methods

### 2.1 Preparation Method

The synthesis of ZnO nanoparticles was performed following the method of Kakiuchi *et al.* [12]. A mixture of 100 mL aqueous solution containing zinc acetate dehydrated 0.05 M and urea 1.0 M was prepared. The pH of the solution was adjusted to 4.9 by using several drops of concentrated acetic acid. The mixture was filled in a Teflon autoclave (150 mL), and the hydrothermal synthesis of ZnO proceeded at 80 °C for 15 hours in a constant temperature. After the hydrothermal reaction, the obtained $Zn(OH)_2$ were thoroughly washed with deionized water and vacuum-dried at 60 °C for several hours. Finally, the $Zn(OH)_2$ powder was treated at 210 °C for 1 hour in the air to obtain the ZnO nanoparticles.

The fabrication of $ZnCo_2O_4$ was done following the sacrificial template accelerated (STAH) method. For the fabrication of the spinel $ZnCo_2O_4$ nanoparticles, the ZnO templates were placed in plastic bottles containing the 50 ml water solution of $Co(NO_3)_2$ (cobalt to zinc molar ratio, $R_{Co/Zn}$=2). The closed bottles were magnetically agitated at room temperature for a day to obtain the highest substitution degree. Afterward, the obtained nanoparticles $ZnCo_2O_4$ were washed with deionized water for several times, then was subjected to vacuum-dry at 50 °C for 60 minutes and calcined in the air at the temperature of approximately 250 °C for 2 hours.

### 2.2 Material Characterization

The elemental composition of the spinel nanoparticles was examined using atomic absorption spectroscopy (AAS). The X-ray diffraction (XRD) patterns of the sample were recorded on a Bruker D8 Advance instrument operating at 40 kV and 40 mA using Cu-Kα radiation (λ = 0.15406 nm). The crystal size values were calculated from the XRD pattern by using Scherrer's equation ($d_{XRD}$). The morphology of the samples was examined by scanning electron microscopy (SEM, FEI Quanta FEG 650 model) and transmission electron microscopy (TEM, JEOL-JEM 2100F). The instrumental contribution to line broadening was taken into account. The Raman spectra were recorded on a micro-Raman spectrophotometer (JASCO Raman NRS-3000) using a 633 nm excited laser at room temperature. The BET specific surface

area of the samples was estimated by means of $N_2$ adsorption isotherms (-196 °C) obtained on a Micromeritics ASAP 2020 analyser. Analysis of the isotherms in the relative pressure range of 0.04-0.20. Ex-situ X-ray photoelectron spectroscopy (XPS) was carried out on a Specs spectrometer, using Al-Kα (30 eV) radiation emitted from a double anode. The binding energies of the resulting spectra were corrected with the binding energy of adventitious carbon (284.6 eV) in the C1s region. The backgrounds were corrected by Shirley baselines.

### 2.3. Photocatalytic Tests

The photocatalytic activity tests under visible irradiation were performed with a 400W NAV 4Y lamp combined with a 400 nm UV cut-off filter. The photodegradation test was kept at room temperature using a cooling water circulation.

20 mg of $ZnCo_2O_4$ photocatalyst mixed with 50 mg/L of MB (300 mL) and the suspension was stirred in the dark for 2 hours before light irradiation, to make sure that an adsorption-desorption equilibrium was obtained. The concentration of MB after equilibration was measured and taken as initial concentration ($C_0$) to release the adsorption in the dark.

During the light irradiation, 5 mL of a suspension was collected every 30 minutes, centrifuged and the concentration of MB solution (with concentration $C$) was measured by UV-vis spectrophotometer. The $ZnCo_2O_4$ catalyst was collected right after the photocatalytic test finishing and thoroughly washed by deionized water. It was then vacuum-dried for several hours at 60 °C. For the cycle stability test, the photocatalyst was tested in 10 reaction stages using the same amount of photocatalyst at the same photocatalysis test condition (total reaction time: 3300 hours).

## 3. Results and Discussion

### 3.1 Fabrication of $ZnCo_2O_4$ Catalysts

The sacrificial template accelerated hydrolysis (STAH), a novel hard exo-templating technique that consists of the formation of metal oxide nanostructures via the hydrolysis of metal ions in the vicinity of a ZnO template [23-26]. The protons $H^+$ were formed during the hydrolysis of the metal ions, which simultaneously dissolve the ZnO scaffold, leading to the precipitation of the metal hydroxides. The unique characteristic of STAH method is the simultaneous dissolution of the ZnO template during the hydrolysis of the substituted metal cation [23]. Liu *et al.* have fabricated $MnO_2$-NiO tubular arrays through a sacrificial template accelerated hydrolysis by using non-polar ZnO as a template at hydrothermal condition [27]. The common of all these works is that the ZnO template is made of nanowires or nanorods with less polar characteristics and the product after the synthesis is metal oxides which are in the form of metal oxide nanotubes. Newly, Vu *et al.* have demonstrated that the ZnO template with high polarity can be used for the fabrication of a variety of metal oxides supported on the same micromesh with very high values of specific surface area [23]. On the other hand, for values of *p*Ka over -9.5 (strongly and mildly acidic cations) the basic synthesis method allowed for the complete substitution to take place, and metal oxides with purities over 95% and high yields were obtained. And for weakly acidic cations, in case of $Co^{2+}$, with values of pKa below around -9.5, only partial substitutions were achieved, which conducts to the formation of mixed oxides [23].

$ZnCo_2O_4$ samples were synthesized in this work following a sacrificial template accelerated hydrolysis procedure (STAH), using the ZnO nanoparticles with high polarity as a template.

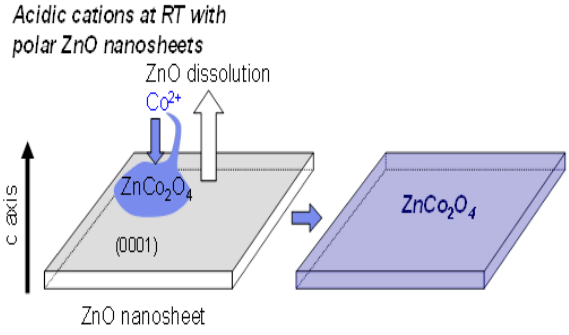


**Figure 1.** The formation of $ZnCo_2O_4$ using STAH method

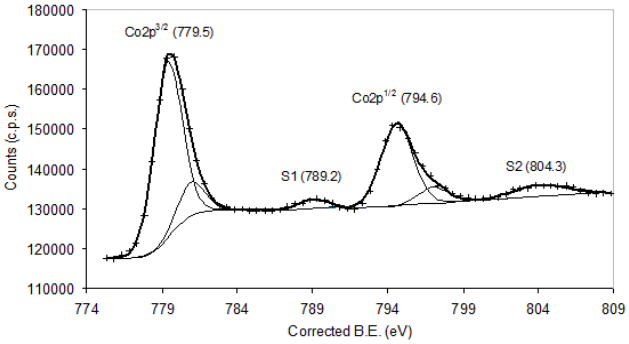


**Figure 2.** XPS Co2p region for Co spinel sample

The synthesis scheme was presented in Figure 1. The elemental analysis results (AAS) represent the molar ratio between Co and Zn $R_{Co/(Co+Zn)}$ which is 0.6 as the maximum. It could be explained by the fact that there is an only partial substitution to form spinel $ZnCo_2O_4$ nanoparticles [23,28,29].

### 3.2 Oxidation State of Cobalt in the Spinel

In order to check the valence state of the spinel metal oxide, XPS technique was employed. Figure 2 shows the Co2p region for the $ZnCo_2O_4$ sample prepared in this work. We already know that the determination of the oxidation states of Co cations is quite problematic because similar spectra of binding energy of Co2p peaks can be obtained for CoO, $Co_3O_4$, and $Co_2O_3$ oxides. Therefore, the information of the satellite peaks is useful to determine the oxidation state of Co cations. Some studies have demonstrated that the energy gap between the Co2p main peak and the satellite peaks can give a piece of relevant information about the oxidation states [30]. When the energy gap is approximately 6.0 eV, the Co cations valence will be $2^+$. The valence of Co cations will $3^+$ when the energy gap has a value of 9-10 eV.

As observed in Figure 2 the energy gaps between the satellites (S1 and S2) and the main peaks are 9.6 and 9.5 eV for $Co2p^{3/2}$ and $Co2p^{1/2}$ regions respectively, thus confirming that the oxidation state of cobalt in our sample is +3 [21,31]. Furthermore, the peak for $Co2p^{3/2}$ and $Co2p^{1/2}$ in this work is good agreement with the written date informed to $Co^{3+}$ [32].

### 3.3. Structure and Compositional Analysis

Figure 3 shows the X-ray diffraction peaks for different samples of $ZnCo_2O_4$. The wurtzite diffraction peaks of ZnO at 32° were disappeared after the synthesis. This indication signifies that ZnO was completely consumed. As shown in Figure 3, all the diffraction peaks can be indexed to $ZnCo_2O_4$. It should be noted here that the XRD spectrum of the $ZnCo_2O_4$ shows a peak shifting of about 0.35° to lower angles to that of the reference $ZnCo_2O_4$ (PDF# 00-023-1390). The result might be a consequence of a higher macro-strain of the sample prepared in this work at low temperature (250 °C), which may result in a higher lattice parameter. The particle size obtained by using the Scherrer equation is 4.1±0.6 nm (TEM inspection shows particles with sizes of 4 nm).

To ensure the structure obtained in this work, Raman spectroscopy of metal mixed oxide is shown in Figure 4 to determine the structure of the spinel metal oxide. Pure ZnO template was also measured for the comparison. As

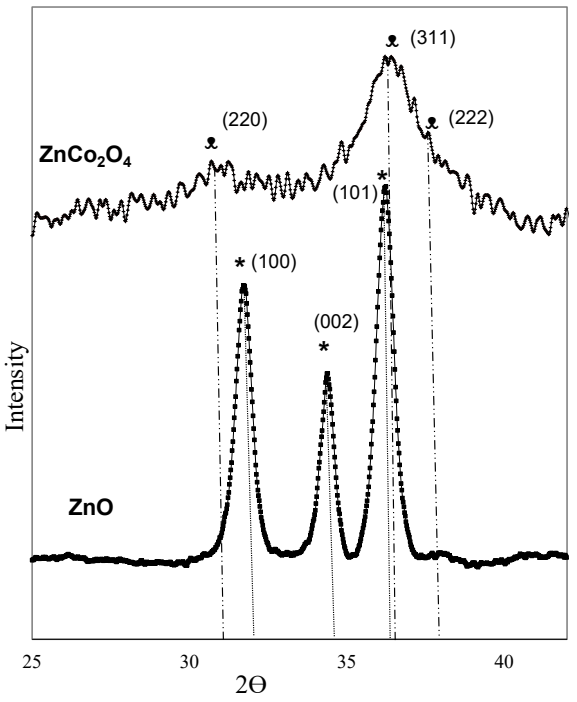


**Figure 3**. XRD patterns of the ZnO template and spinel $ZnCo_2O_4$

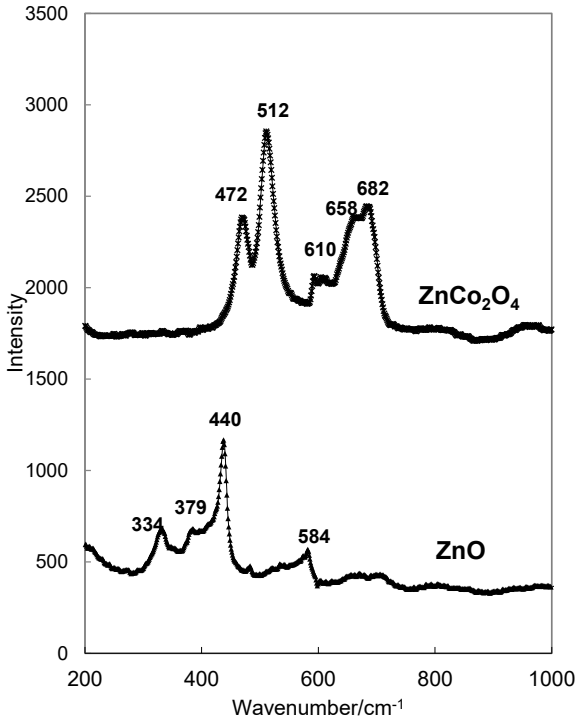


**Figure 4.** Raman patterns of the ZnO template and spinel $ZnCo_2O_4$

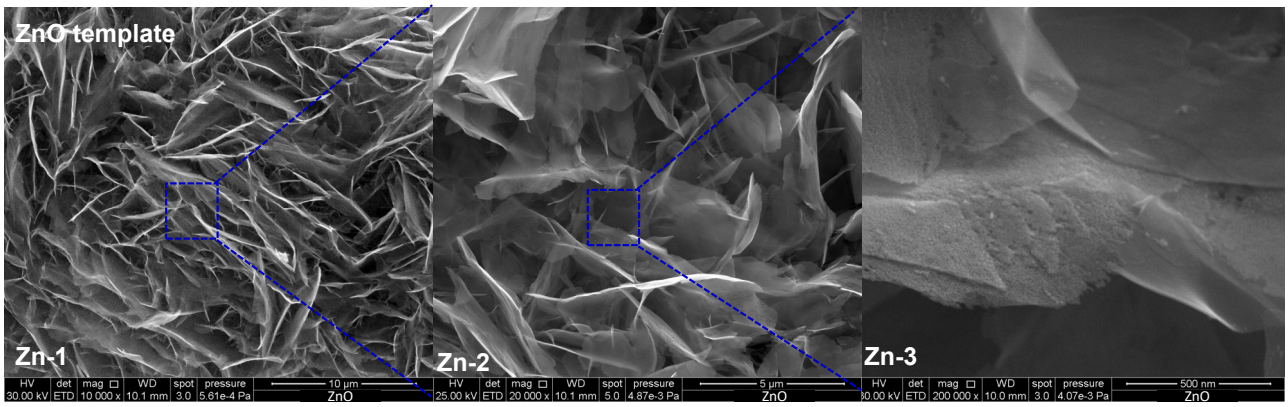


**Figure 5.** SEM images of the ZnO template

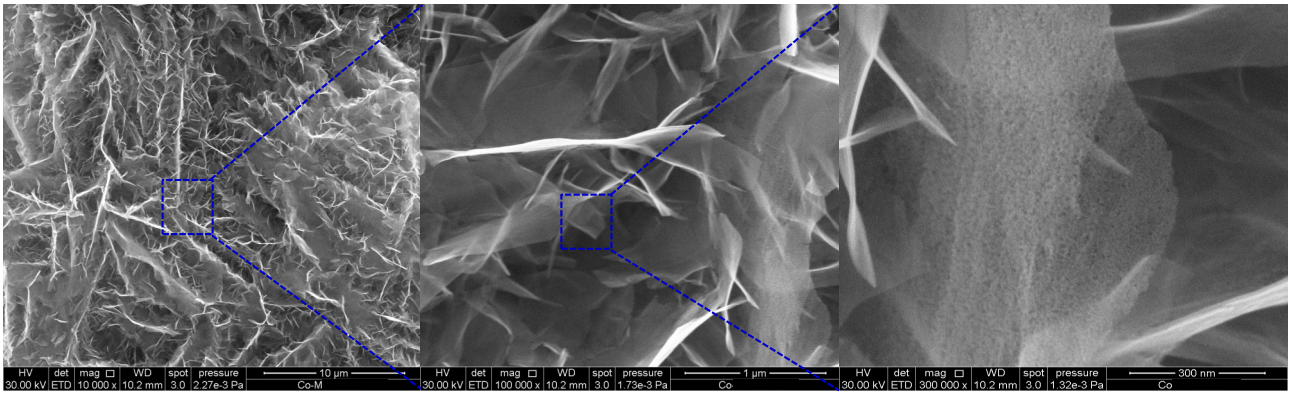

**Figure 6.** SEM images of spinel $ZnCo_2O_4$

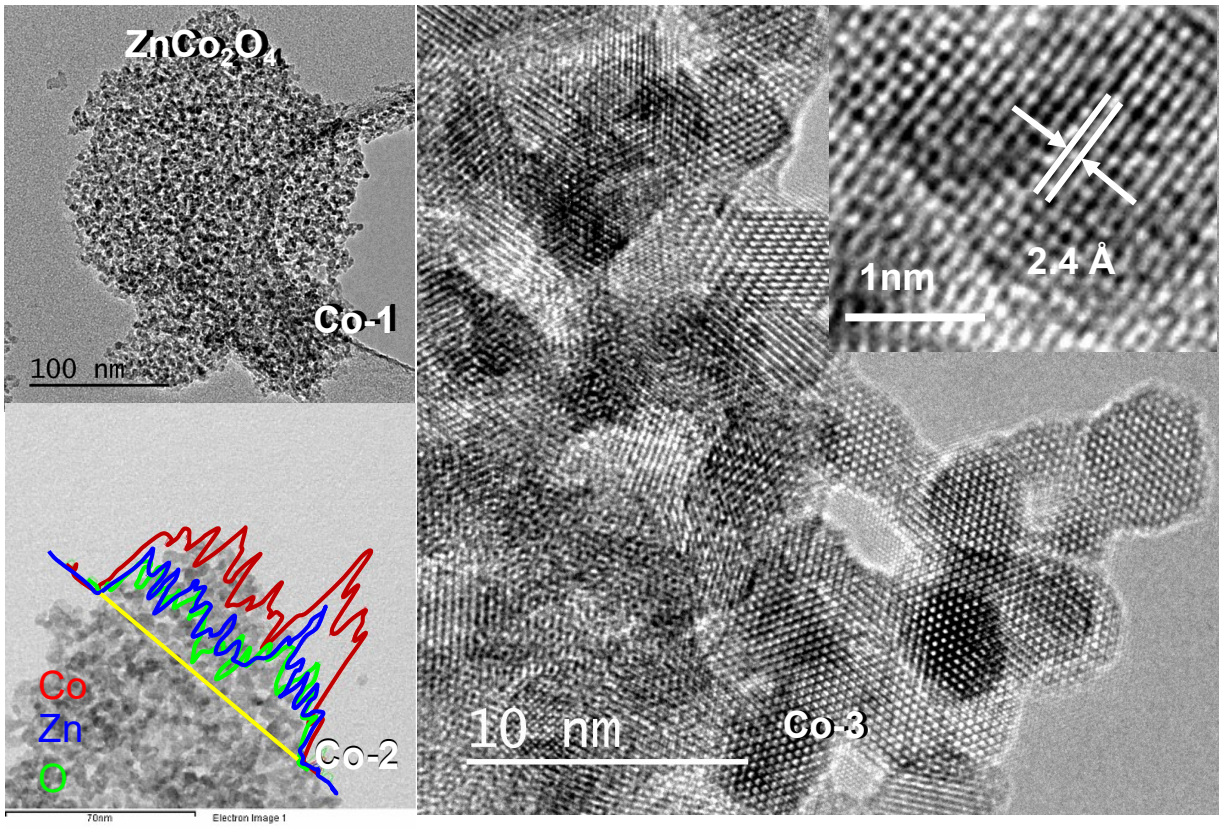


**Figure 7.** TEM images of spinel $ZnCo_2O_4$

observed in Figure 4, the relatively high intensities of 466 $cm^{-1}$ and 508 $cm^{-1}$ are compared to that of 681 $cm^{-1}$, indicate to the presence of $ZnCo_2O_4$. It can be concluded that the ZnO was wholly converted into $ZnCo_2O_4$ using STAH method.

3.4 Size, Morphology, and Specific Surface Area of the Spinel

The morphology, particle size and chemical information of the obtained spinel were analyzed by SEM (Figure 5 and Figure 6) and EDX- assisted TEM (Figure 7). Figure 5 shows the original morphology of the ZnO template. As observed, the general morphology of the initial ZnO template is nearly maintained after the substitution process, which was shown in Figure 6. The spinel $ZnCo_2O_4$ nanoparticles consist of thin sheets with a homogenous distribution in the range 5-7 μm (Figure 6). The nanosheets are grouped of several units which are randomly distributed in the volume of the micro-petal flower.

Also, typical TEM images of spinel metal mixed oxide replicated from corresponding ZnO scaffold were given (Figure 7). These interconnected nanograins provide the high porosity of the nanosheets. Figure 7 shows that the nanosheets are grouped by a nanoparticles of $ZnCo_2O_4$ with sizes of 4 nm which is in good agreement with the crystal sizes calculated by XRD. Moreover, Figure 7 shows the lattice

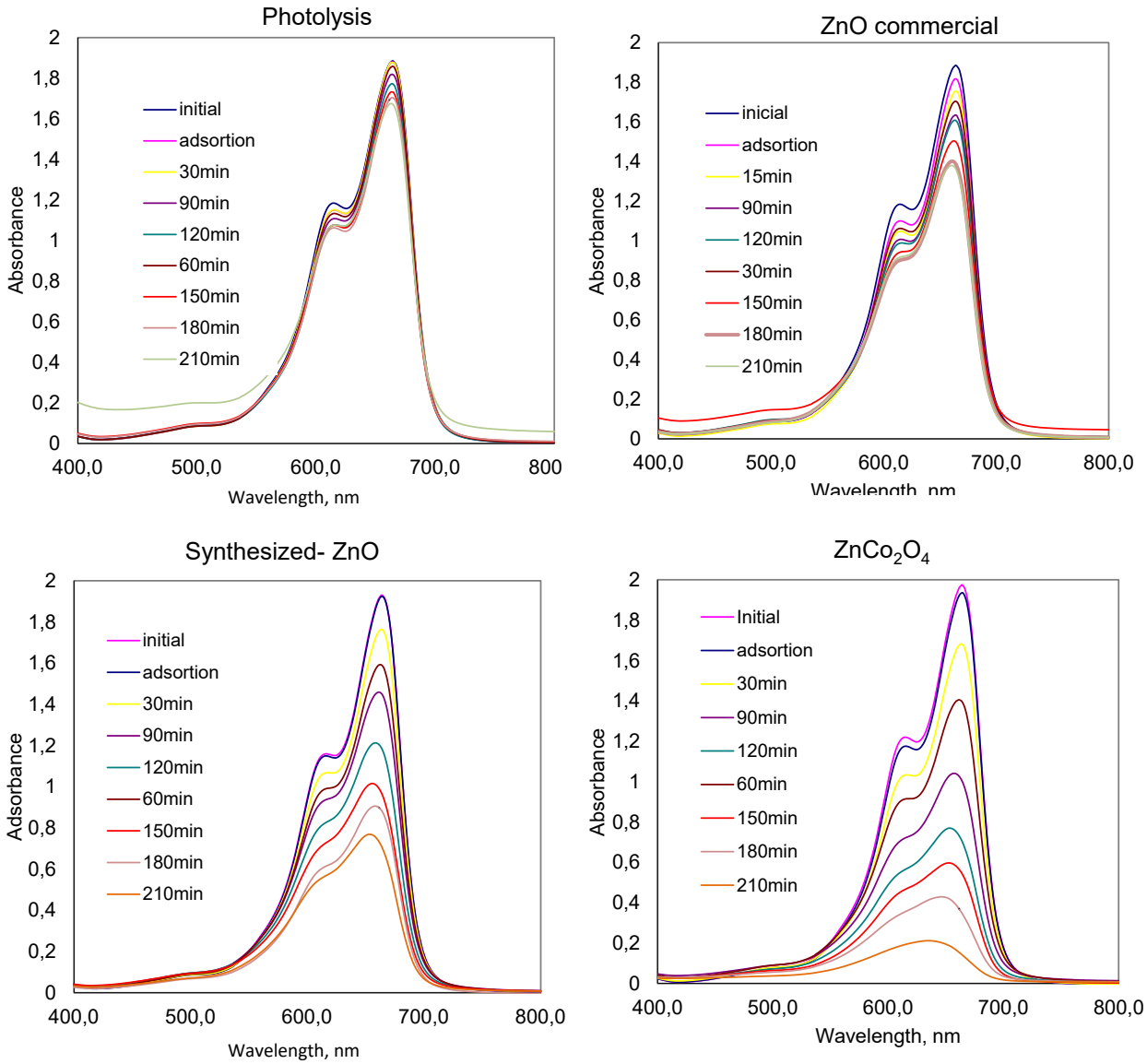


**Figure 8.** UV-Vis spectra of MB at different time intervals in presence of different photocatalyst: Photolysis, ZnO commercial, synthesized ZnO template, $ZnCo_2O_4$

fringe plane of the obtained $ZnCo_2O_4$. The clear lattice fringe with a spacing of 2.4 Å can be observed, which corresponds to the (220) planes of the cubic spinel structure $ZnCo_2O_4$.

The composition of $ZnCo_2O_4$ was analyzed using a dispersive X-ray spectroscopy (EDS) line scan profile of Co, Zn, and O (Figure 7). The observed uniform distribution of the two respective metal Co-Zn on the nanoparticle which demonstrates that there is a homogenous distribution of Co and Zn with a ratio atom approximately Co/Zn = 0.6. This result is fairly agreed with the result of elemental analysis (AAS).

$N_2$ sorption measurements show that these spinel $ZnCo_2O_4$ nanoparticles generally have high BET surface areas of 178 $m^2/g$, pore size distribution maximum of 2-100 nm (Table 1). The value of specific surface area of the spinel obtained is higher than that of the original ZnO template. The result may be due to the controlled growth of the metal hydroxide nuclei inside the electrostatic field of the polar ZnO surface [23].

### 3.5 Photocatalytic Activity of the $ZnCo_2O_4$ Catalysts

The photocatalytic activity of $ZnCo_2O_4$ nanoparticles was studied for methylene blue (MB) degradation using visible light. The absorption spectra of MB solution after different irradiation times in the presence of catalysts are shown in Figure 6. In the absence of a catalyst, the absorption intensity of MB has no significant change, even up to 210 minutes (3 hours 30 minutes). These results show that MB is relatively stable to visible light. Meanwhile, when $ZnCo_2O_4$ nanoparticles are added, the intensity of absorption peaks at 664 nm decreases dramatically during irradiation time which means that MB degradation has occurred. The photocatalytic test is finished within 210 minutes, demonstrating that $ZnCo_2O_4$ nanoparticle can capably degrade MB under visible light.

Figure 8 exhibits photocatalytic degradation curve of MB with different photocatalyst: no catalyst, ZnO commercial, synthesized ZnO template, $ZnCo_2O_4$ synthesized in this work using STAH method. The $C_0$ and $C$ are initial concentration (after adsorption step) and residue concentration of MB after irradiation time, respectively.

The photocatalytic activities of the commercial ZnO nanoparticles, synthesized ZnO in this work by Vu method [12], $ZnCo_2O_4$ synthesized in this work using STAH method were also performed under the same test conditions. The results show that the commercial ZnO and the template synthesized ZnO in this work degrade approximately 27 and 60%, respectively, of MB in 210 minutes. And the synthesized $ZnCo_2O_4$ nanoparticles show complete degradation of MB solution in 210 minutes and demonstrate the outstanding photocatalytic activity comparing with the synthesized template ZnO and even the ZnO commercial material.

Figure 9 shows the graph of $\ln(C/C_0)$ versus reaction time. The graph presents a linear relationship, showing first-order kinetics of the

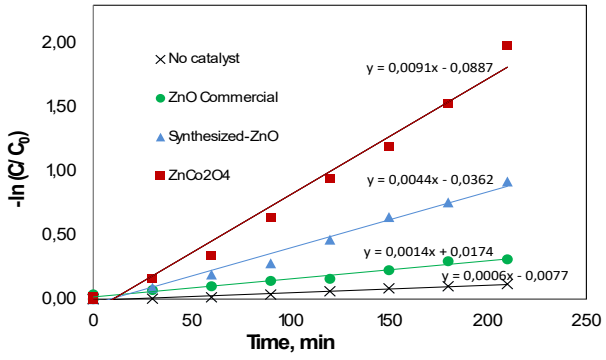


**Figure 9.** The plots of $\ln(C_0/C)$ against illumination time for degradation of MB in presence of different photocatalysts

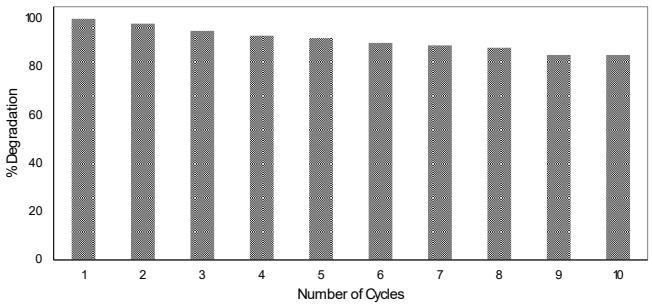


**Figure 10.** The stability test of the photocatalyst $ZnCo_2O_4$ under visible light.

**Table 1.** Physical properties of the synthesized $ZnCo_2O_4$ [23]

| Materials | $S_{BET}$, $m^2/g$ | Pore size, maxima, nm | Crystal size, nm, XRD | Crystal size, nm, TEM |
|---|---|---|---|---|
| ZnO | 80 | 16;109 | 13 | 11 |
| $ZnCo_2O_4$ | 178 | 2; 100 | 4 | 4 |

degradation of MB under visible light. The rate constants were determined as: 0,0014; 0,044; 0,0091 $min^{-1}$ for commercial ZnO, synthesized ZnO template and $ZnCo_2O_4$, respectively. The order of rate constants is as follows: $ZnCo_2O_4$ > synthesized ZnO template > commercial ZnO. The BET surface areas of the commercial ZnO, synthesized ZnO, $ZnCo_2O_4$ nanoparticles are 40, 80, and 178 $m^2/g$ [12]. Small crystal size always gives a large specific surface area which enhances the visible light photocatalytic capacity.

Stability test of $ZnCo_2O_4$ was realized by repeating the degradation of MB for ten times using the recovered photocatalyst after each cycle. The data obtained were shown in Figure 10, showing that there is a slight decrease in photocatalytic activity of $ZnCo_2O_4$ during a long time reaction. This result indicates that $ZnCo_2O_4$ is highly stable photocatalyst at visible light and it can be reusable for several stages. This opens a new route for the treatment of dye using photocatalyst under visible light.

## 4. Conclusions

In this study, we reported for the first time the synthesis of $ZnCo_2O_4$ nanoparticles by using ZnO with highly polar as an initial template according to STAH method. The obtained $ZnCo_2O_4$ nanoparticles shown a higher surface area in comparison to the initial ZnO template. The photocatalytic activity of $ZnCo_2O4$ under visible irradiation was investigated by the degradation of MB. The photodegradation of MB follows pseudo-first order kinetics over all the tested catalysts: commercial ZnO, ZnO template, and $ZnCo_2O_4$. The $ZnCo_2O_4$ showed the highest catalytic activity in the visible region due to its small crystal size, and large specific surface area. The $ZnCo_2O_4$ catalyst is also highly stable and can be used as a photocatalyst repetitively without photocorrosion effect. The results open a new route for the investigation of the degradation of dye in the visible light.

## Acknowledgements

The work was supported by Hanoi University of Science and Technology through the project T2017-TT-009.

## References

[1] Ibhadon A., Fitzpatrick, P. (2013). Heterogeneous Photocatalysis: Recent Advances and Applications, *Catalysts*, 3: 189-218.

[2] Kabra, K., Chaudhary, R., Sawhney, R.L. (2004). Treatment of Hazardous Organic and Inorganic Compounds through Aqueous-Phase Photocatalysis: A Review, *Ind. Eng. Chem. Res.*, 43: 7683-7696.

[3] Geckeler, K.E., Volchek, K.(1996). Removal of Hazardous Substances from Water Using Ultrafiltration in Conjunction with Soluble Polymers, *Environ. Sci. Technol*., 30: 725-734.

[4] Shitu, A. (2014). Removal of Methylene Blue Using Low Cost Adsorbent: A Review, *Research journal of chemical Sciences*, 4: 2231-606.

[5] Schneider, J., Matsuoka, M., Takeuchi, M., Zhang, J., Horiuchi, Y., Anpo, M., Bahnemann, D.W. (2014). Understanding $TiO_2$ Photocatalysis: Mechanisms and Materials», *Chem. Rev.*, 114: 9919-9986.

[6] Lazar, M.A., Varghese , S., Nair, S.S. (2012). Photocatalytic water treatment by titanium dioxide: recent updates, *Catalyst*, 2: 572-601.

[7] Hamid, S.B., Teh, A.S.J., Lai, C.W. (2017). Photocatalytic Water Oxidation on ZnO: A Review, *Catalysts*, 7: 93-99.

[8] Ong, C.B., Ng, L.Y., Mohammad, A.W. (2018). A review of ZnO nanoparticles as solar photocatalysts: Synthesis, mechanisms and applications, *Renewable and Sustainable Energy Reviews*, 81: 536-551.

[9] Kansal, S.K., Ali, A.H., Kapoor, S. (2010). Photocatalytic decolorization of biebrich scarlet dye in aqueous phase using different nanophotocatalysts, *Desalination*, 259: 147-155.

[10] Podporska-Carroll, J., Mylesa, A., Quilty, B., Mc Cormack, D.E., Fagan, R., Hinder, S.J., Dionysiou, D.D., Pillai, F.C. (2017). Antibacterial properties of F-doped ZnO visible light photocatalyst, *Journal of Hazardous Materials*, 324: 39-47.

[11] Banerjee, S., Pillai, S.C., Falaras, P., O'Shea, K.E., Byrne, J.A., Dionysiou, D.D. (2014). New Insights into the Mechanism of Visible Light Photocatalysis, *J. Phys. Chem. Lett.* 5: 2543-2554.

[12] Vu, T.T., Valdés-Solis, T., Marbán, G. (2013). Fabrication of wire mesh–supported ZnO photocatalysts protected against photocorrosion. *Applied Catalysis B: Environmental*. 140–141: 189-198.

[13] Xiao, F.X. (2012). Construction of Highly Ordered ZnO-$TiO_2$ Nanotube Arrays (ZnO/TNTs) Heterostructure for Photocatalytic Application, *ACS Appl. Mater. Interfaces*, 4: 7055-7063.

[14] Aliaga, J., Cifuentes, N., Gonzalez, G., Sotomayor-Torres, C., Benavente, E. (2018). Enhancement Photocatalytic Activity of the Heterojunction of Two-Dimensional Hybrid Semiconductors ZnO/$V_2O_5$, *Catalyst*, 8(9): 374.

[15] Kandjani, A.E., Sabri, Y.M., Periasamy, S.R., Zohora, N., Amin, M.H., Nafady, A., Bhargava, S.K. (2015), Controlling core/shell formation of Nanocubic p-$Cu_2O$/n-ZnO toward enhanced photocatalytic performance, *Langmuir*, 31: 10922-10930.

[16] Feng, Y., Wang, G., Liao, J., Li, W., Chen, C., Li, M., Li, Z. (2017). Honeycomb-like ZnO Mesoporous Nanowall Arrays Modified with Ag Nanoparticles for Highly Efficient Photocatalytic Activity, *Scientific Reports*, 7: 11622.

[17] Zhang, H., Zong, R., Zhu, Y. (2018). Photocorrosion Inhibition and Photoactivity Enhancement for Zinc Oxide via Hybridization with Monolayer Polyaniline, *J. Phys. Chem. C.,* 113: 4605–4611.

[18] Fageria, P., Gangopadhyay, S., Pande, S. (2014). Synthesis of ZnO/Au and ZnO/Ag nanoparticles and their photocatalytic application using UV and visible light, *RSC Adv.*, 4: 24962-24972.

[19] Zhang, Y., Xu, J., Xu, P., Zhu, Y., Chen, X., Yu, W. (2010). Decoration of ZnO nanowires with Pt nanoparticles and their improved gas sensing and photocatalytic performance, *Nanotechnology*, 21: 285501.

[20] Cousin, P., Ross, R.A. (1990). Preparation of Mixed Oxides-A Review, *Materials Science and Engineering: A*, 130:119-125.

[21] Zhang, H., Zong, R., Zhu, Y. (2017). Defective $ZnCo_2O_4$ with Zn vacancies: Synthesis, property and electrochemical application, *Journal of Alloys and Compounds,* 724:1149–1156.

[22] Cui, B., Lin, H., Zhao, X., Li, J.B., Li, W.-D. (2011). Visible Light Induced Photocatalytic Activity of $ZnCo_2O_4$ Nanoparticles», *Acta Physico-Chimica Sinica*, 27: 112-120.

[23] Vu, T.T., Marbán, G. (2014). Sacrificial template synthesis of high surface area metal oxides. Example: An excellent structured Fenton-like catalyst, *Applied Catalysis B: Environmental,* 152–153: 51-58.

[24] Liu, J., Jiang, J., Bosman, M., Fan, H.J. (2012). Three-dimensional tubular arrays of $MnO_2$-NiO nanoflakes with high areal pseudocapacitance, *J. Mater. Chem.*, 22: 2419-2426.

[25] Liu, J., Li, Y., Fan, H., Zhu, Z., Jiang, J., Ding, R., Hu,Y., Huang, X. (2012). Iron Oxide-Based Nanotube Arrays Derived from Sacrificial Template-Accelerated Hydrolysis: Large-Area Design and Reversible Lithium Storage, *Chem. Mater,* 22: 212–217.

[26] Zeng, W., Zheng, F., Li, R., Zhan, Y., Li, Y., Liu, J. (2012). Template synthesis of $SnO_2$/α-$Fe_2O_3$ nanotube array for 3D lithium ion battery anode with large areal capacity, *Nanoscale*, 4: 2760-2765.

[27] Liu, J., Jiang, J., Bosman, M., Fan, H.J. (2012). Three-dimensional tubular arrays of $MnO_2$–NiO nanoflakes with high areal pseudocapacitance, *J. Mater. Chem.*, 22(6): 2419-2426.

[28] Vu, T.T., Rodil, A.B., Marbán, G., Valdés-Solís, T. (2014). Nanostructured stainless steel wire mesh-supported $Cd_xZn_{1-x}O$: A stable photocatalyst under visible and ultraviolet irradiation, *Journal of Environmental Chemical Engineering*, 2: 1612-1620.

[29] Vu, T.T., Valdés-Solís, T., Marbán, G. (2014). Novel high surface area stainless steel wire mesh supported $Ni_{0.7}Zn_{0.3}O$ solid solution prepared by room temperature sacrificial template accelerated hydrolysis. Application in the production of hydrogen from methanol. *Applied Catalysis B: Environmental*, 160–161: 57–66.

[30] Wei, W., Chen, W., Ivey, D. (2008). Rock Salt−Spinel Structural Transformation in Anodically Electrodeposited Mn−Co−O Nanocrystals, *Chem. Mater.*, 20: 1941-1947.

[31] Klevak, E., Kas, J.J., Rehr, J.J. (2014). Charge transfer satellites in x-ray spectra of transition metal oxides, *Physical Review B*, 89(8): 085123.

[32] Hu, L., Qu, B., Li, C., Chen, Y., Mei, L., Lei, D., Chen, L., Li, Q., Wang, T. (2013). Facile synthesis of uniform mesoporous $ZnCo_2O_4$ microspheres as a high-performance anode material for Li-ion batteries, *J. Mater. Chem. A*, 18: 5596-5602.